

# Construction of an Immunophenoscore-Related Signature for Evaluating Prognosis and Immunotherapy Sensitivity in Ovarian Cancer

Haonan Jiang, Guzhanuer Awuti, and Xiaoqing Guo\*



Cite This: *ACS Omega* 2023, 8, 33017–33031



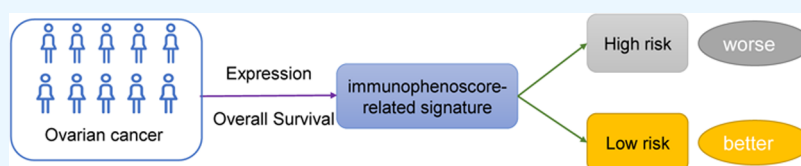
Read Online

ACCESS |

Metrics & More

Article Recommendations

Supporting Information



**ABSTRACT:** Ovarian cancer (OC) is the deadliest gynecological malignancy in the world, and immunotherapy is emerging as a promising treatment. Immunophenoscore (IPS) is a robust biomarker distinguishing sensitive responders from immunotherapy. In this study, we aimed to construct a prognostic model for predicting overall survival (OS) and identifying patients who would benefit from immunotherapy. First, we combined The Cancer Genome Atlas (TCGA) and The Cancer Immune Atlas (TCIA) data sets and incorporated 229 OC samples into a training cohort. The validation cohort included 240 OC samples from the Gene Expression Omnibus (GEO) cohort. The training cohort was divided into high- and low-IPS subgroups to obtain differentially expressed genes (DEGs). DEGs with OS were identified by Univariate Cox regression analysis. The least absolute shrinkage and selection operator (LASSO) Cox regression was used to construct the prognostic model. Then, immune and mutation analyses were performed to explore the relationship between the model and the tumor microenvironment (TME) and tumor mutation burden (TMB). Eighty-three DEGs were obtained between the high- and low-IPS subgroups, where 17 DEGs were associated with OS. The five essential genes were selected to establish the prognostic model, which showed high accuracy for predicting OS and could be an independent survival indicator. OC samples that were divided by risk scores showed distinguished immune status, TME, TMB, immunotherapy response, and chemotherapy sensitivity. Similar results were validated in the GEO cohort. We developed an immunophenoscore-related signature associated with the TME to predict OS and response to immunotherapy in OC.

## INTRODUCTION

Ovarian cancer (OC) is one of the most common gynecological malignancies and has the highest mortality.<sup>1</sup> Traditional treatment options for OC include surgical resection, chemotherapy based on platinum, and targeted therapy containing vascular endothelial growth factor (VEGF) inhibitors.<sup>2</sup> Olaparib targeted for breast cancer gene (BRCA) mutation has widely been used in the population and achieves satisfactory effects.<sup>3</sup> Although combining previous treatments could improve overall survival (OS) in OC, the 5-year survival rate remains low at 40%.<sup>4</sup> There are no better strategies for treating advanced and recurrent OC; therefore, further research on this matter is urgently needed.

OC is an immunogenic tumor infiltrated with intratumoral T cells.<sup>5</sup> Immunotherapy has recently gained significant attention among populations, improving survival outcomes, as validated by some large-scale clinical trials.<sup>6–12</sup> In contrast to traditional therapies, immunotherapy exerts antitumor effects by enhancing self-immunity, including immune checkpoint inhibitors, adoptive T-cell therapy, and cancer vaccines.<sup>13</sup> Unfortunately, not all patients respond well to immunotherapy, so exploring a new prognostic marker for evaluating survival value and

making immunotherapy more rational in OC patients is urgent.

The Cancer Immune Atlas (TCIA) showed determinants of immunogenicity and developed an immunophenoscore (IPS) for solid tumors based on machine learning.<sup>14</sup> IPS is a robust predictor for response to immunotherapy with cytotoxic T lymphocyte antigen-4 (CTLA-4) and programmed cell death protein 1 (PD-1) blockers, verified in two cohorts treated with anti-CTLA-4 and anti-PD-1 in melanoma,<sup>15,16</sup> which comprises four classes: effector cells, suppressive cells, major histocompatibility complex (MHC) molecules, and immunomodulators. However, the IPS is an excellent biomarker for identifying responders to immunotherapy and is not a good survival predictor for OC patients. Therefore, we constructed a prognostic model based on the IPS that reflects the sensitive

Received: July 6, 2023

Accepted: August 15, 2023

Published: August 30, 2023



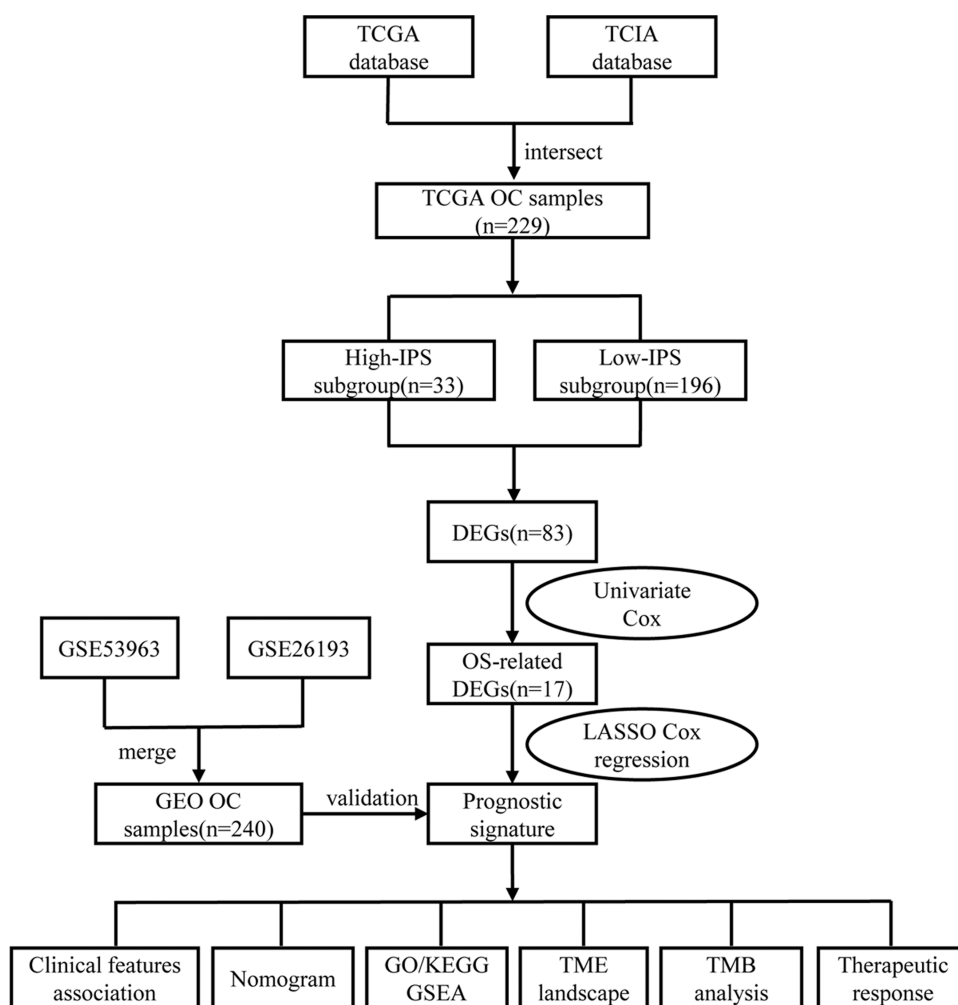


Figure 1. Workflow of this research.

response to immunotherapy and predicts survival outcomes in OC patients.

## RESULTS

**Identification of IPS-Related Genes.** Figure 1 presents the workflow. First, we integrated the OC samples from the Cancer Genome Atlas (TCGA) OC cohort and TCIA data set and obtained 229 OC samples. IPS is a crucial predictor of immunotherapy response, so we divided TCGA OC samples into two subgroups based on the median IPS: the IPS-high and IPS-low groups. Eighty-three differentially expressed genes (DEGs) with  $\text{adj. } p < 0.05$  and  $|\log_2\text{foldchange}| > 0.5$  were identified when we compared samples with a better response with those with a worse response to immunotherapy in the TCGA OC cohort (Figure 2A). Among them, 63 genes were upregulated in the high-IPS subgroup, while 20 genes were downregulated. Univariate Cox regression analysis was performed to identify DEGs associated with OS in OC. We found that 17 DEGs were related to OS ( $p < 0.05$ ), where 2 DEGs were harmful to OS with a hazard ratio (HR)  $> 1$ , while 15 DEGs were beneficial for OS with  $\text{HR} < 1$  (Figure 2B). Venn diagram, network correlation, and heatmap showed the overlapping genes with different expression levels and OS-related prognostic values (Figure 2C–E). The least absolute shrinkage and selection operator (LASSO) Cox regression was performed to determine the most representative genes for

reflecting OS, and five genes were obtained (Figure 2F–G), which consisted of the prognostic model (Table S2). Based on the coefficient and expression of these genes, the risk scores were calculated as follows:  $\text{risk score} = (0.016 \times \text{GLIS2}_{\text{expression}}) + (-0.065 \times \text{ISG20}_{\text{expression}}) + (-0.140 \times \text{HLA-DOB}_{\text{expression}}) + (-0.208 \times \text{KRTCAP3}_{\text{expression}}) + (-0.005 \times \text{OCIAD2}_{\text{expression}})$ .

**Prognostic Value of the 5-Gene Signature.** To estimate the generality of the prognostic model constructed from the TCGA OC cohort, we adopted a validation cohort merged by GSE53963 and GSE26193. The risk score of the two cohorts was calculated using the former formula. We considered the median risk score of the TCGA cohort as the cutoff, dividing OC samples into low- and high-risk subgroups. Principal component analysis (PCA) showed that two subgroups were two distinctive clusters (Figure 3A,B). A receiver operating characteristic (ROC) curve was generated to evaluate the sensitivity and specificity of the prognostic model, and the area under the curve (AUC) was 0.68 for one year, 0.69 for three years, and 0.67 for five years in the TCGA cohort (Figure 3C).

Moreover, the AUC was 0.62 for one year, 0.62 for three years, and 0.63 for five years in the GEO cohort (Figure 3D). The distribution of risk scores and survival status validated that the high-risk group had worse survival outcomes and shorter survival times in both cohorts (Figure 3E,F). Kaplan–Meier

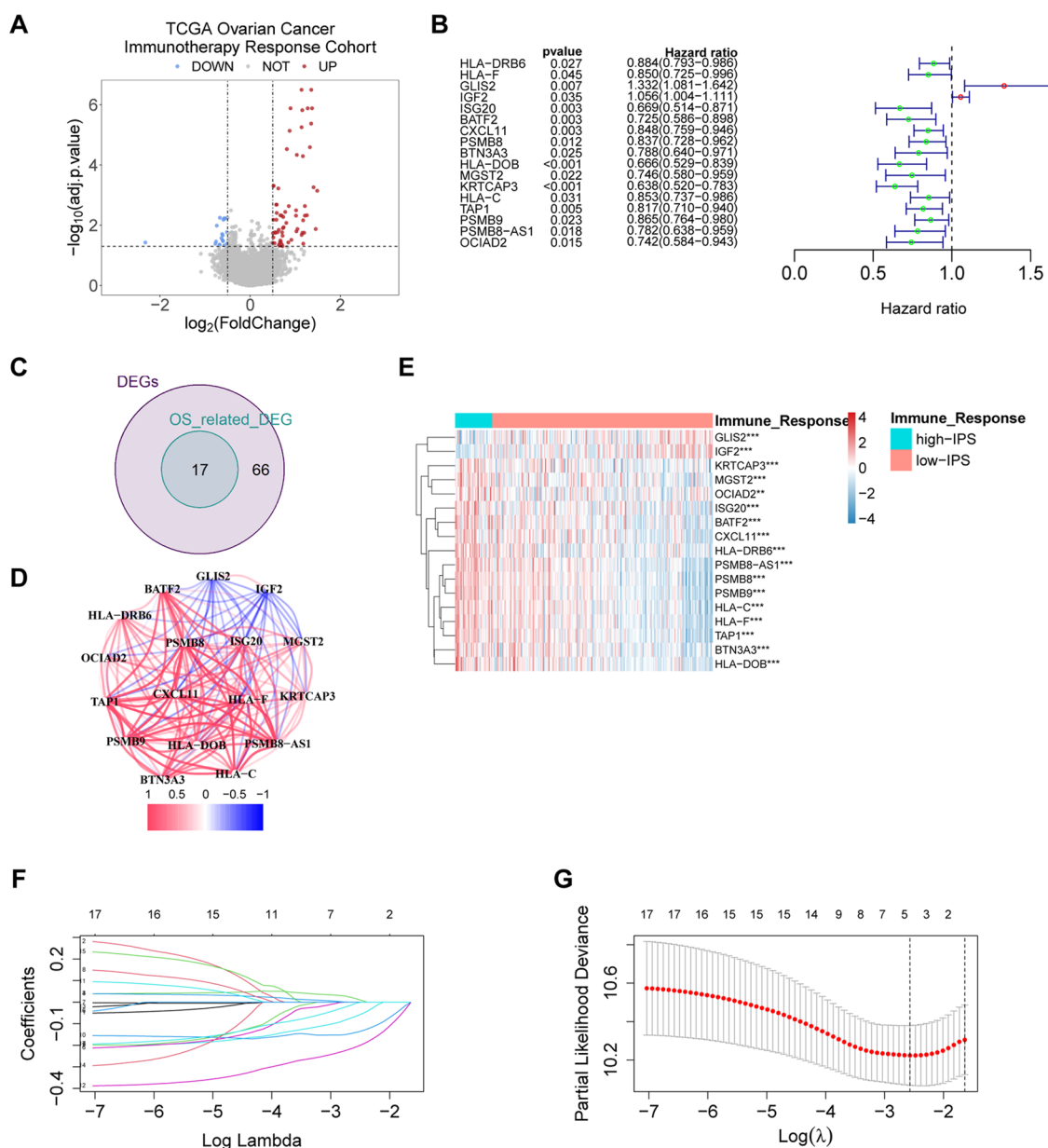


**Figure 2.** Identifying prognostic DEGs between the high- and low-IPS subgroups. (A) The downregulated and upregulated DEGs are shown in the volcano plot; red dots represent upregulated DEGs, and blue dots represent downregulated DEGs. (B) Univariate Cox regression analysis identified 17 prognostic DEGs. (C) The overlapping genes are shown in the Venn diagram. (D, E) The association and expression of these genes are displayed in the network and heatmap. (F) LASSO coefficient profiles of the genes. (G) Coefficients profile plot with the  $\log(\lambda)$  sequence for selecting the best  $\lambda$ . \* $p < 0.05$ , \*\* $p < 0.01$ , \*\*\* $p < 0.001$ , \*\*\*\* $p < 0.0001$ ; ns, no significance.

analysis also demonstrated that lower risk scores contributed to better OS in both cohorts (Figure 3G,H).

**Correlation between Prognostic Model and Clinical Features.** We explored the relationship between the prognostic model and clinical features, including age, grade, and clinical stage. Patients over 60 years old were recognized as elderly. The elderly population showed a higher risk score. However, no significant differences in risk scores were found in grade and clinical stages (Figure 4A–C). The GEO cohort showed a higher risk score in late clinical stages III–IV (Figure S1A,B). Additionally, univariate and multivariate Cox regression analyses demonstrated that the risk score was an independent survival factor for OS (Figure 4D,E, hazard ratio (HR) = 5.432, 95% confidence interval (CI) = 2.704–10.909,  $p < 0.001$ ). Similarly, the GEO cohort validated that the risk

score served as an independent survival element (Figure S1C,D, HR = 2.013, 95% CI = 1.134–3.571,  $p = 0.017$ ).

**Nomogram for Predicting Survival.** According to the clinicopathological features and risk scores, we constructed a nomogram to predict the possibility of OS more accurately for both cohorts (Figure 5A,B). High points indicate worse survival outcomes in the nomogram. Subsequently, the time-dependent ROC curve was conducted to demonstrate a highly accurate nomogram for predicting survival, showing that the AUC was 0.713 for one year, 0.641 for three years, and 0.620 for five years in the TCGA cohort (Figure 5C). In the GEO cohort, AUC was 0.621 for one year, 0.658 for three years, and 0.710 for five years (Figure 5D). The calibration curve also showed that the OS calculated by the nomogram was generally in accordance with the actual OS (Figure 5E,F).

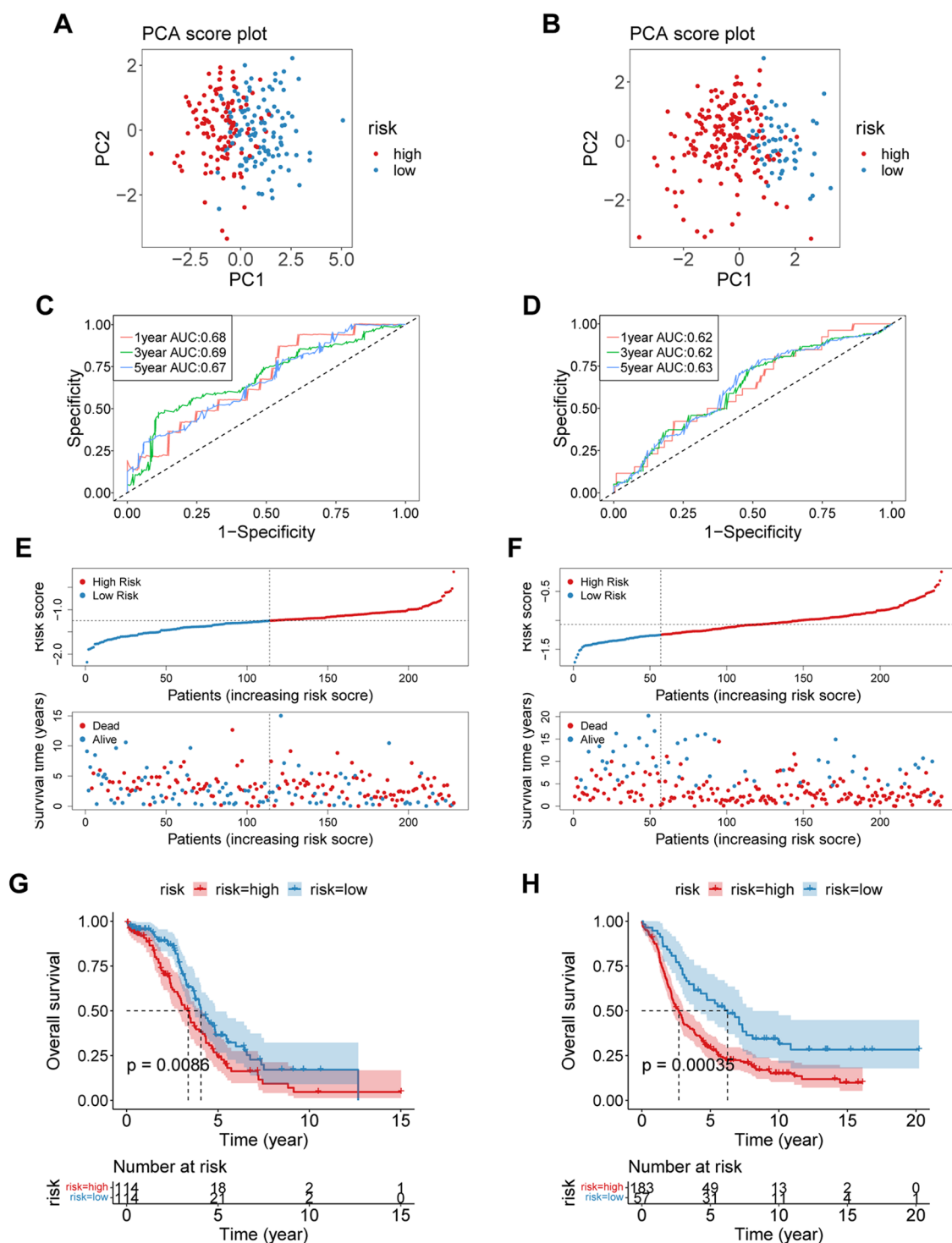


**Figure 3.** Construction of a 5-gene signature for prognosis. (A, B) The PCA score plot shows the distribution of samples divided into high- and low-risk subgroups in the TCGA cohort and Gene Expression Omnibus (GEO) cohort. (C, D) ROC curve of the prognostic model in the TCGA cohort and GEO cohort. (E, F) The distribution of survival status in the TCGA cohort and GEO cohort. (G, H) Survival analysis between the high- and low-risk subgroups in the TCGA cohort and GEO cohort.

**Functional Enrichment Analysis.** To understand how the prognostic model influenced OC progression and led to longer OS, we explored gene function and pathway differences between the high- and low-risk subgroups via Gene Ontology (GO) and Kyoto Encyclopedia of Genes and Genomes (KEGG) enrichment analyses. The GO analysis suggested that DEGs mainly participated in the plasma membrane signaling receptor complex, regulation of T-cell activation, and

antigen binding (Figure 6A–C). In addition, KEGG analysis showed that DEGs were enriched in cell adhesion molecules and antigen processing and presentation (Figure 6D). Moreover, gene set enrichment analysis (GSEA) revealed the molecular mechanism, where the immunoreactive pathways, such as antigen processing and presentation pathways, were primarily enriched in the low-risk subgroup. However, the high-risk subgroup exhibited activation of the mitogen-

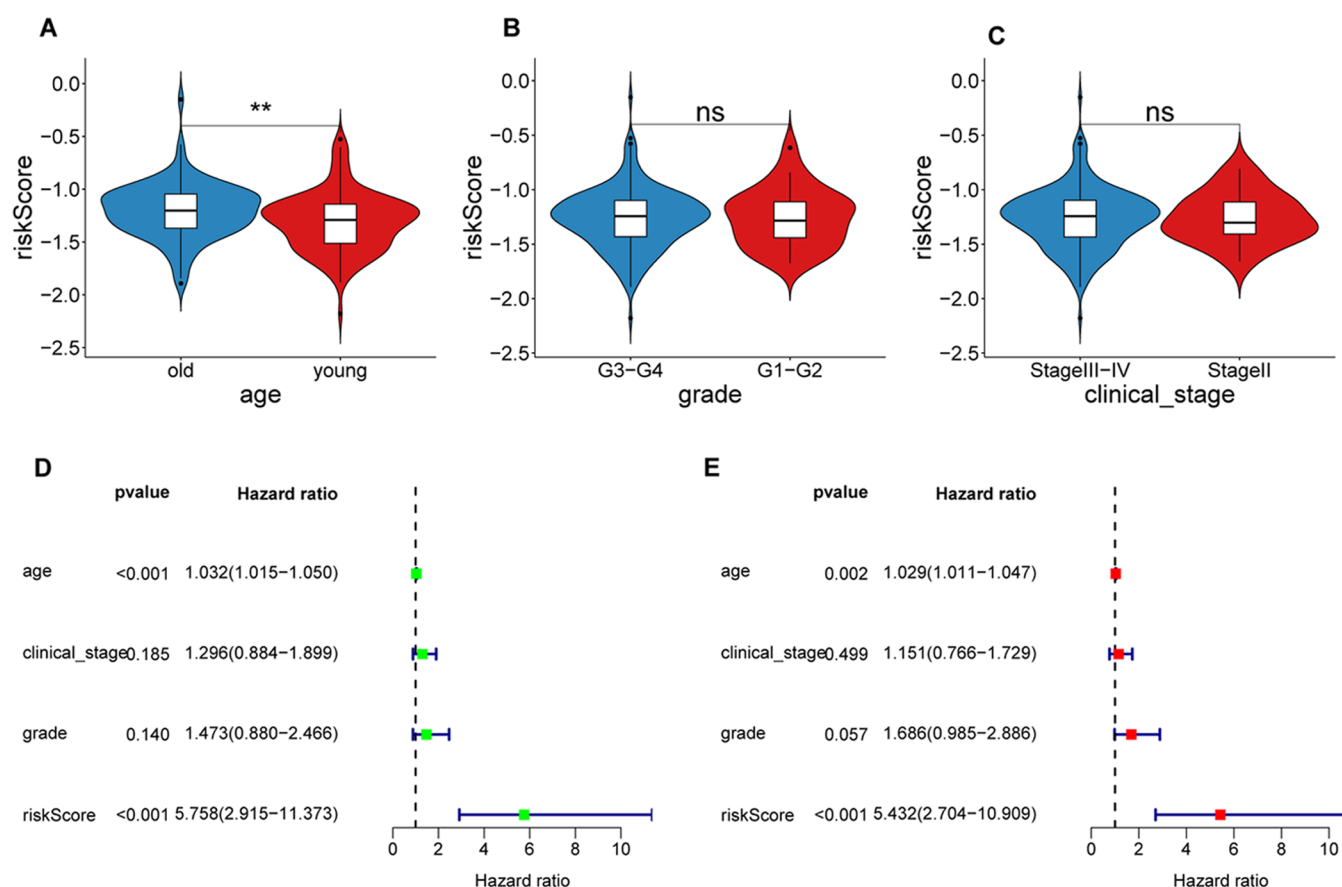


**Figure 4.** Association between clinical features and the prognostic model. (A–C) Relationship between the prognostic model and different clinical elements, including age, grade, and clinical stages. (D, E) Univariate and multivariate Cox regression analyses for the prognostic model and other clinical features in the TCGA cohort.

activated protein kinase (MAPK) and focal adhesion signaling pathways (Figure 6E). Similar results were obtained in the GEO cohort (Figure S2A–E). The immune-related pathways were mainly enriched in the low-risk subgroup to influence tumor progression.

**Immune Landscape of Prognostic Model.** The TME, including stromal and immune cells, is crucial in tumor progression, therapeutic effects, and survival outcomes.<sup>17</sup> We explored whether the prognostic model could shape the TME to influence tumor clearing.

The heatmap shows the differences in the immunological landscape between the high- and low-risk subgroups (Figure 7A). The estimation of stromal and immune cells in malignant tumor tissues using the expression data (ESTIMATE) algorithm was used to calculate the immune score, ESTIMATE score, tumor purity, and stromal score. As shown in Figure 7B, the low-risk subgroup exhibited significantly higher ESTIMATE and immune scores and lower tumor purity scores. Moreover, immunological activities and immune cells scored higher in the low-risk subgroup (Figure 7C,D). We also analyzed the tumor immune landscape of the GEO cohort, and similar results were obtained. Low-risk subgroup exhibited higher immune scores and immunological activities (Figure S3A–G).

An antitumor response consists of several vital steps. We further explored the relationship between the risk score and antitumor response based on the Tracking Tumor Immunophenotype (TIP) meta-server. We found that most steps

scored higher in the low-risk subgroup (Figure 7E), demonstrating that the low-risk subgroup might exert a more robust immune response.

**Association with Tumor Mutation Burden.** Tumor mutation burden (TMB) is associated with immunotherapy response and produces new tumor antigens to attract tumor-specific T cells,<sup>18</sup> so we calculated the TMB of each OC sample. Low-risk subgroup showed higher TMB (Figure 8A,B), and high TMB contributed to better OS in the TCGA OC cohort (Figure 8C). Combining TMB and risk score, patients with high TMB and low risk showed the longest survival time (Figure 8D). Then, the mutation landscapes of the high- and low-risk subgroups were distinguished in waterfall plots (Figure 8E). The top 15 mutated genes in OC were tumor protein 53 (TP53), titin (TTN), mucin 16 (MUC16), sushi multiple domains 3 (CSMD3), neurofibromatosis type 1 (NF1), topoisomerase II $\alpha$  (TOP2A), usherin (USH2A), hemicentin-1 (HMCN1), FAT atypical cadherin 3 (FAT3), ryanodine receptor 2 (RZR2), mucin 17 (MUC17), filaggrin (FLG), microtubule actin crosslinking factor 1 (MACF1), apolipoprotein B (APOB), and breast cancer-associated gene 1 (BRCA1). A missense mutation was the most common somatic mutation type. The mutation frequency was higher in the low-risk subgroup (96.34%) than in the high-risk subgroup (91.03%). Samples with low risk exhibited a higher mutation frequency of TTN and lower mutation frequency of TP53 than the high-risk subgroup.

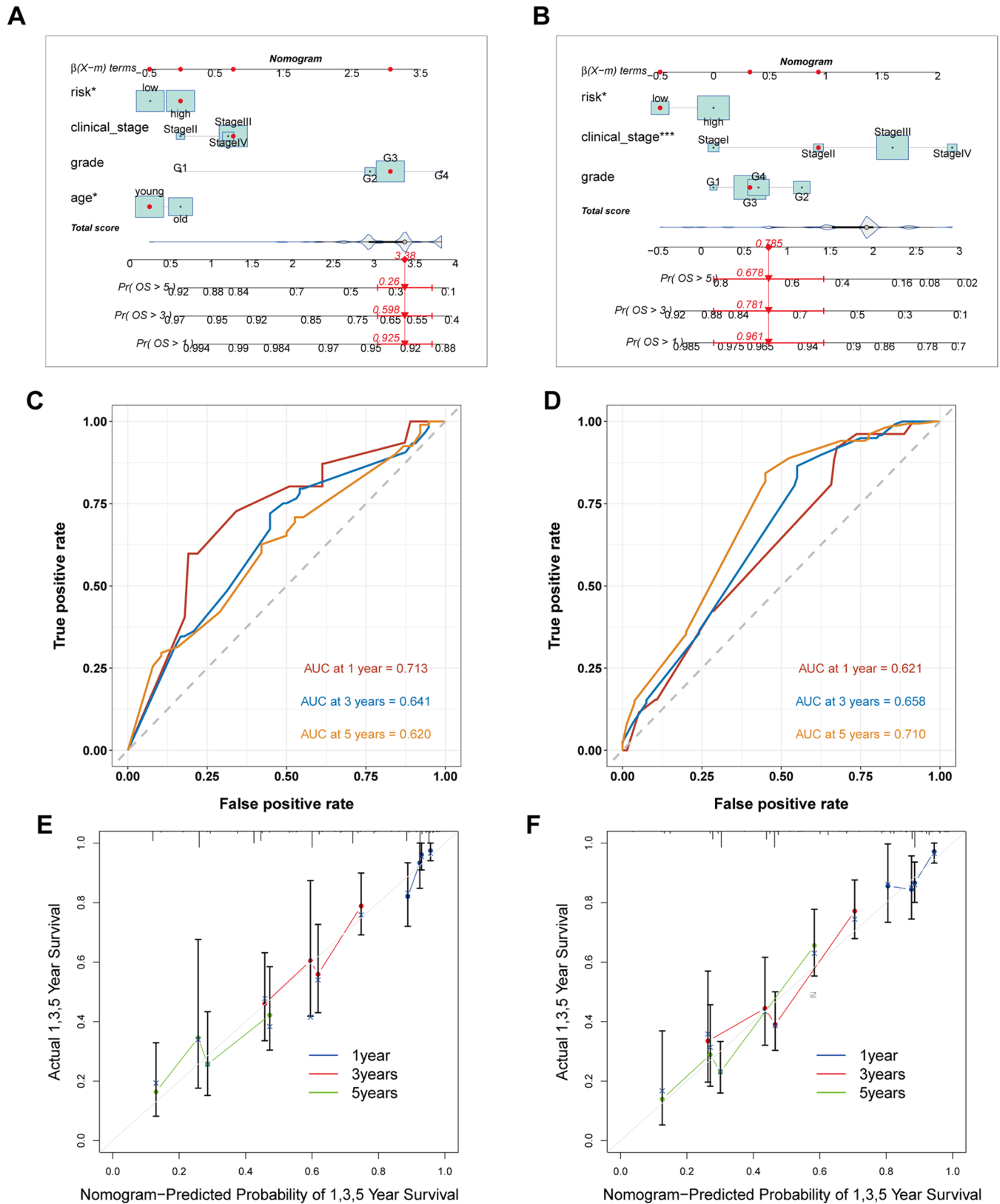


**Figure 5.** Construction and evaluation of the nomogram. (A, B) The nomogram for predicting the survival probability of OC patients combines clinical features and risk scores in the TCGA and GEO cohorts. (C, D) The ROC curve and (E, F) calibration plots of the nomogram for predicting OS for one year, three years, and five years in the TCGA cohort and GEO cohort.

**Therapeutic Response of the Prognostic Model.** High TMB contributed to a better response to immunotherapy.<sup>19,20</sup> Previous studies implied that the low-risk subgroup exhibited

higher TMB with better survival. Therefore, we explored the expression of immune checkpoints between the high- and low-risk subgroups. We found that the expression of immune

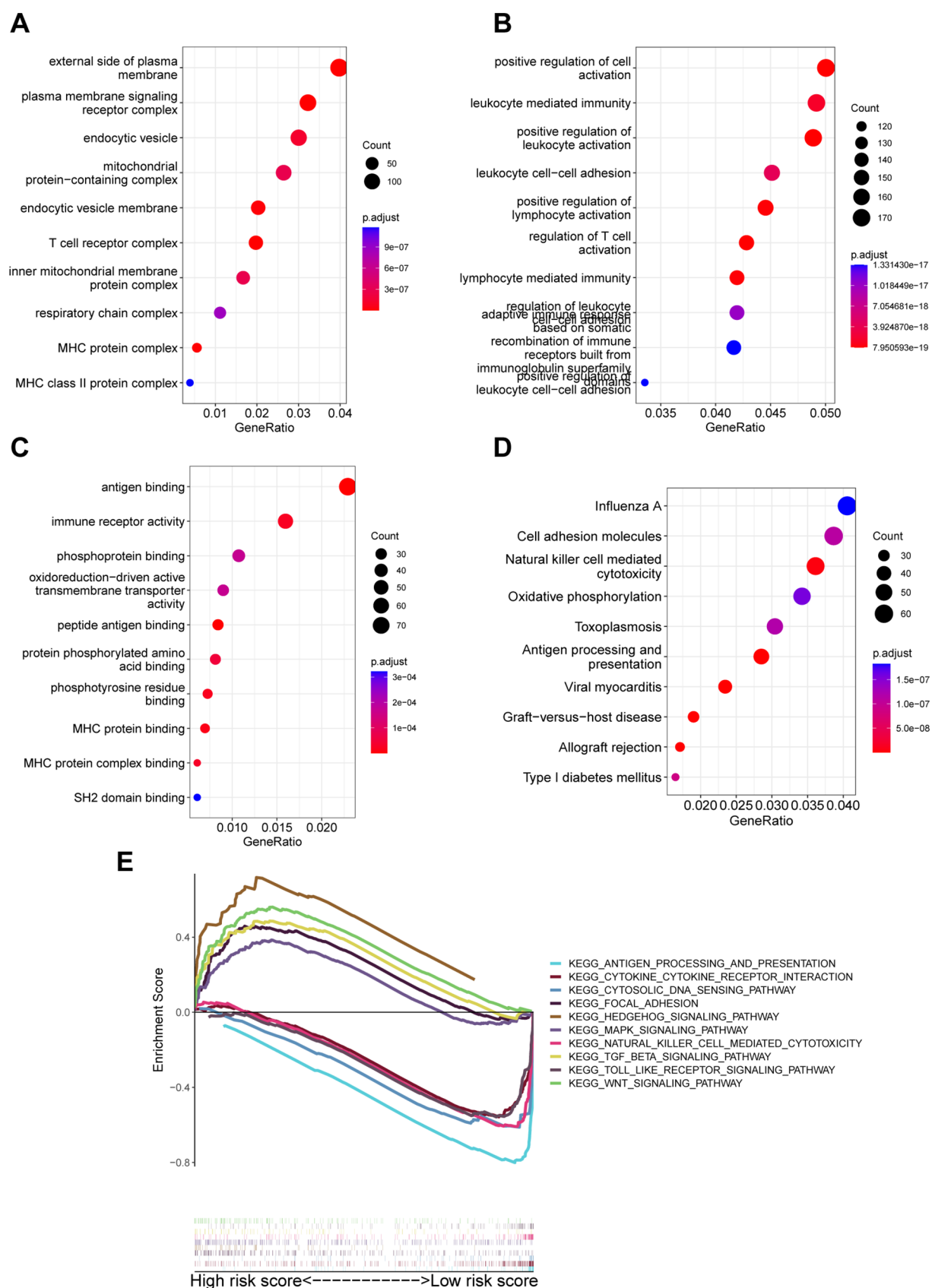


**Figure 6.** Functional analysis of DEGs between the high- and low-risk subgroups. GO annotation terms of DEGs between the low- and high-risk subgroups for (A) cellular components, (B) biological process, and (C) molecular functions. (D) KEGG enrichment analysis for DEGs between the low- and high-risk subgroups. (E) GSEA findings.

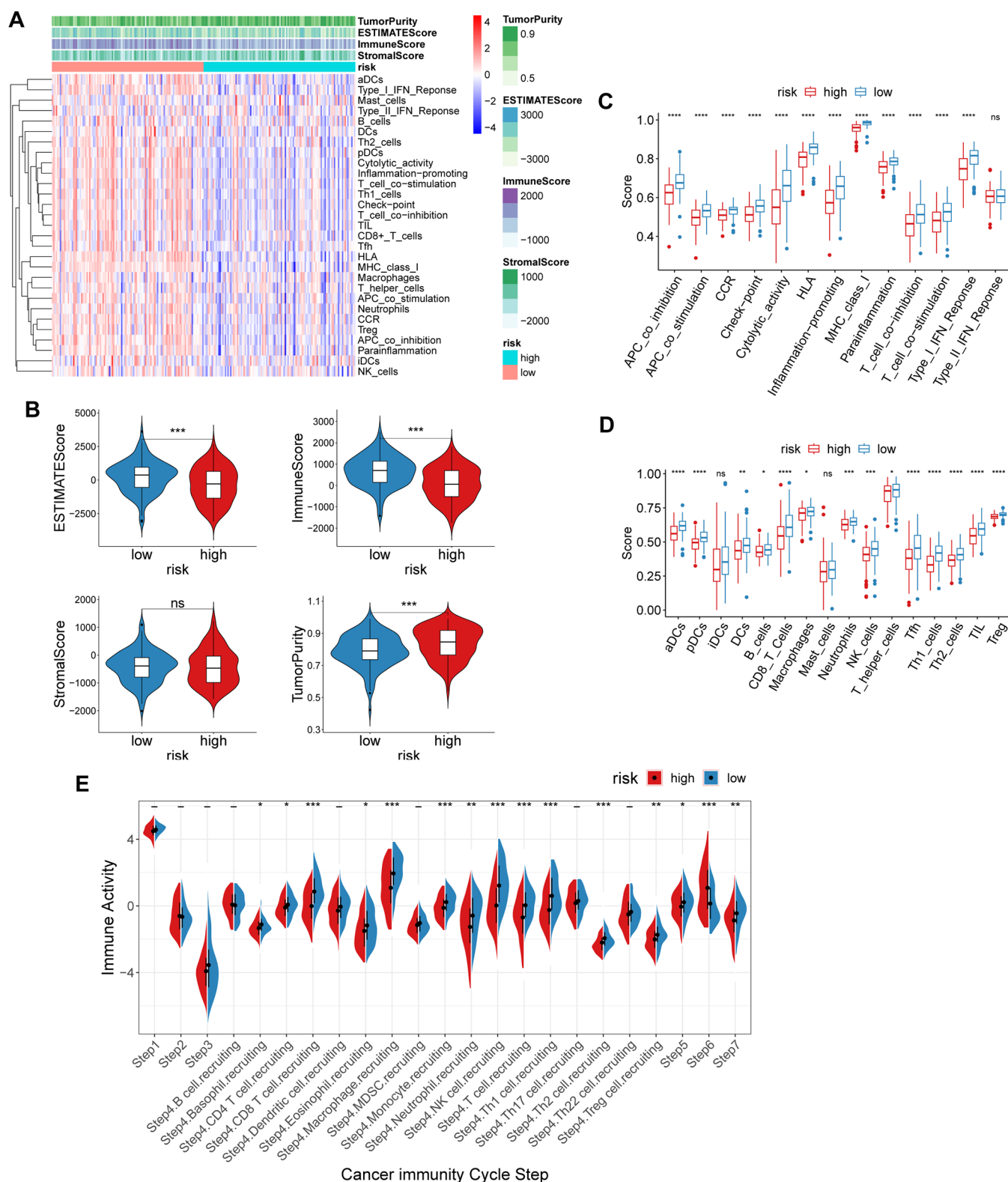


**Figure 7.** Landscapes of the TME between the high- and low-risk subgroups. (A) Heatmap indicates the difference in the TME between the low- and high-risk subgroups. (B) The diversities of the immune score, stromal score, ESTIMATE score, and tumor purity between the low- and high-risk subgroups. (C) The differences in the proportions of 13 immune-related pathways between the low- and high-risk subgroups. (D) The differences in the proportions of 16 immune cells between the low- and high-risk subgroups. (E) The variability of the antitumor steps between the high- and low-risk subgroups. \* $p < 0.05$ , \*\* $p < 0.01$ , \*\*\* $p < 0.001$ , \*\*\*\* $p < 0.0001$ ; ns, no significance.

checkpoints was upregulated in the low-risk subgroup, consistent with pleasing immune treatment effects in the

low-risk subgroup (Figure 9A–D), which was validated in the GEO cohort (Figure S4).

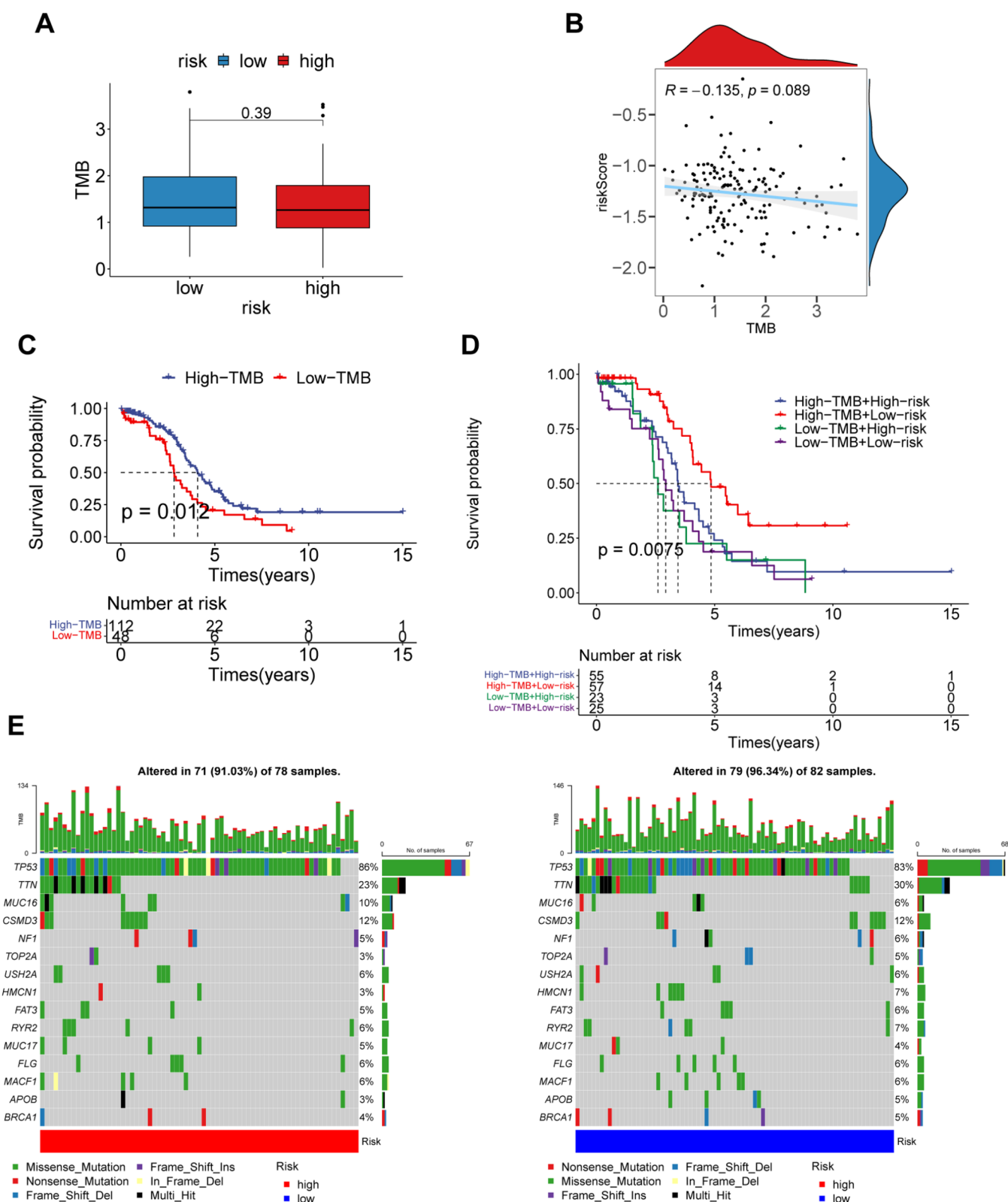


**Figure 8.** Characteristics of TMB in the high- and low-risk subgroups. (A) The differences in TMB between the low- and high-risk subgroups. (B) The association of TMB with a risk score. (C) Kaplan–Meier survival analysis of TMB. (D) Effects of the risk score combined with TMB on OS. (E) Top 15 mutated genes in different subgroups.

We further explored the relationship between the prognostic model and nine common chemical drugs for OC patients, including cisplatin, methotrexate, rapamycin, doxorubicin, bleomycin, erlotinib, gemcitabine, docetaxel, and cytarabine,

via the pRRophetic algorithm. The half-maximal inhibitory concentration ( $IC_{50}$ ) of these agents was compared between the high- and low-risk subgroups. We observed that the low-risk subgroup showed stronger sensitivity to bleomycin and

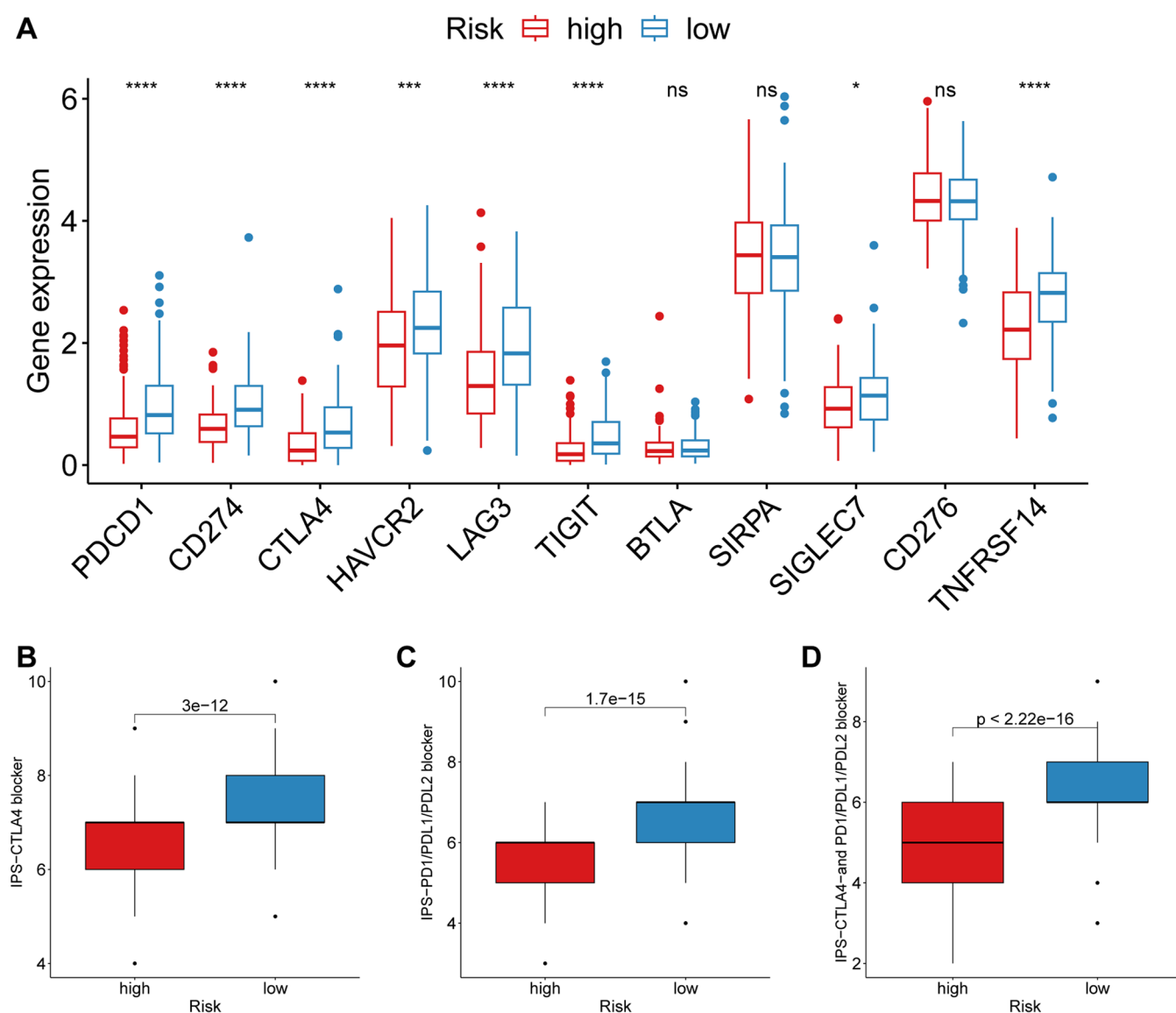


**Figure 9.** Immunotherapeutic responses of the IPS-related signature. (A) Differences in the expressions of immune checkpoints between the low- and high-risk subgroups. (B–D) Comparison of IPS scores in response to immune checkpoint blockers between the low- and high-risk subgroups. \* $p < 0.05$ , \*\* $p < 0.01$ , \*\*\* $p < 0.001$ , \*\*\*\* $p < 0.0001$ ; ns, no significance.

cisplatin. In contrast, the high-risk subgroup showed stronger responses to methotrexate, rapamycin, and erlotinib in the TCGA cohort (Figure 10A–I), which were also analyzed in the GEO cohort (Figure S5A–I).

## DISCUSSION

OC is an immunogenic tumor recognized by host immunity, and intratumoral T cells are positively associated with survival in OC.<sup>21</sup> Harnessing antitumor immunity is a superior option for killing tumor cells, consisting of three key steps, including breaking the immune-suppressive network, identifying tumor antigens, and expanding antigen-specific T cells. IPS is an optimal biomarker to predict patients suitable for immunotherapy, and a higher IPS indicates a more robust immunotherapy response. Therefore, the IPS-related prognostic model could better predict OS and reflect a better response to immunotherapy in OC.

Five genes were used to build the prognostic model, including GLIS2, ISG20, HLA–DOB, KRTCAP3, and

OCIAD2. GLIS family zinc finger 2 (GLIS2) is a TP53-repressing transcription factor that inhibits enhancer activation and promotes colorectal cancer progression.<sup>22</sup> Moreover, overexpression of GLIS2 could cause chemoresistance and poor prognosis of gastric cancer.<sup>23</sup> Interferon-stimulated gene 20 protein (ISG20) is an antiviral protein that inhibits the majority of viruses and its downregulated expression in isocitrate dehydrogenase (IDH2)-mutant glioma is associated with enhanced infiltration of monocyte-derived macrophages and neutrophils, as well as suppression of the adaptive immune response.<sup>24,25</sup> Human leukocyte antigen-DOB (HLA–DOB) is a nonclassical class II molecule that influences the effectiveness of class II-restricted antigen presentation and is involved in macrophage infiltration to influence high-grade serous ovarian carcinoma (HGSOc) survival.<sup>26,27</sup> The DNA methylation profile of keratinocyte-associated protein 3 (KRTCAP3) showed that epigenetic variability influenced the response to the environment in the human population.<sup>28</sup> Ovarian carcinoma immunoreactive antigen-like protein 2 (OCIAD2)

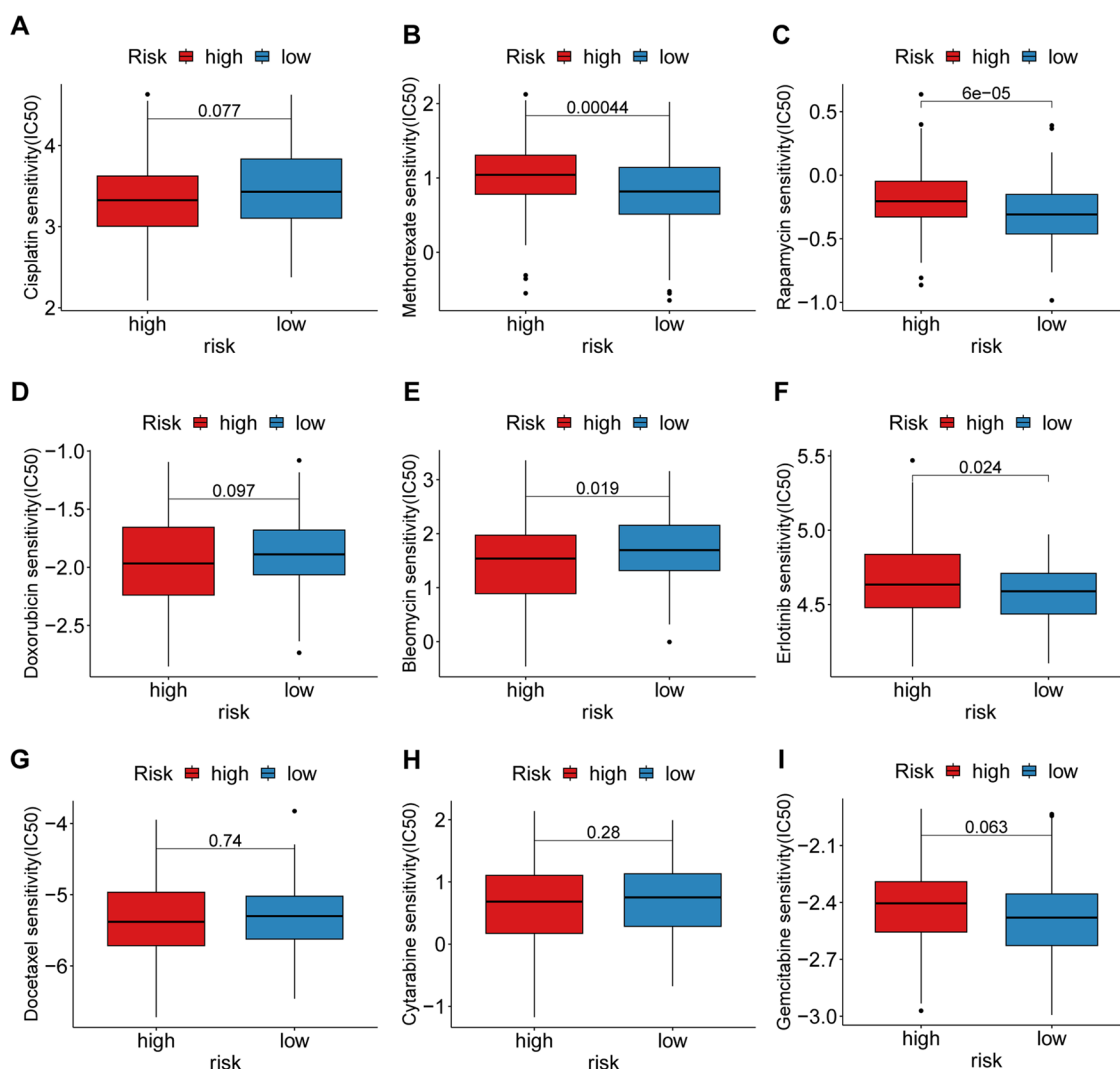


**Figure 10.** Evaluation of the therapeutic response of the IPS-related signature. Sensitivity analysis for (A) cisplatin, (B) methotrexate, (C) rapamycin, (D) doxorubicin, (E) bleomycin, (F) erlotinib, (G) docetaxel, (H) cytarabine, and (I) gemcitabine in OC between the high- and low-risk subgroups.

has been reported to show high immunoreactivity in ovarian tumors and is thought to be a marker for evaluating the malignancy of ovarian mucinous tumors, suppressing tumor proliferation and invasion via the serine/threonine kinase (AKT) pathway in hepatocellular carcinoma.<sup>29,30</sup> In conclusion, these genes all are involved in tumor progression and immunological activities.

Adequate evidence shows the importance of TME in regulating cancer progression and influencing the therapeutic response. Tumor cells can influence the TME to escape host immunity by recruiting immunosuppressive cells and inhibiting the infiltration of immunoreactive cells.<sup>31</sup> Our study demonstrated that the prognostic model was associated with reprogramming the TME, recruiting immune cells, and regulating immunological activities, where antitumor immune cells were mainly enriched in low-risk subgroups, which was beneficial for improving OS.

TMB represents the mutation frequency of cancer, where mutations can produce neoantigens, recognized by effector T cells, harnessing the immune system.<sup>32</sup> To determine whether risk scores regulate the TMB to influence the response to immunotherapy, we compared the gene mutations between the

high- and low-risk subgroups. In the low-risk subgroup, the gene mutation frequency was approximately 96%. Among these genes, TP53 had the highest frequency in the high-risk subgroup, while TTN had the highest frequency in the low-risk subgroup. TTN mutations are correlated with cardiomyopathy and responsiveness to immune checkpoint blockades in solid tumors.<sup>33,34</sup> The satisfactory prognosis of the low-risk subgroup could be due to the higher frequency of TTN mutation.

The immune-suppressive environment is the primary barrier for cancer immunotherapy in OC, even though many tumor-specific CD8<sup>+</sup> T cells accumulate,<sup>35</sup> and the inhibition of immune checkpoint receptors is one of the mechanisms in T-cell function suppression. These receptors negatively modulate T-cell function, including PD-1, CTLA-4, lymphocyte activation gene 3 (LAG-3), T-cell immunoglobulin and mucin domain containing-3 (TIM-3), and T-cell immunoreceptor with immunoglobulin and immunoreceptor tyrosine-based inhibitory motif domains (TIGIT).<sup>36–40</sup> We found that the expression of immune checkpoints was upregulated in the low-risk subgroup, where the low-risk subgroup showed a positive response to immunotherapy in OC. Moreover,

patients with different risk scores showed various sensitivities to agents. The high-risk subgroup exhibited more sensitivity to rapamycin and methotrexate, while bleomycin responded well in the low-risk subgroup.

Although promising results have been achieved, our study still has some limitations. First, the findings were all based on retrospective public cohorts. A prospective study is required to validate the prognostic value of the 5-gene prognostic model. Second, comprehensive experiments are essential to detect the function of the 5 genes in OC and understand the mechanism of the prognostic model.

## CONCLUSIONS

In summary, we constructed a new prognostic model based on the IPS to evaluate the population suitable for immunotherapy and forecast the survival possibility in OC. TME and TMB analyses were performed to explore the potential factors affecting the response to immunotherapy. This model could aid in more rational decision-making regarding immunotherapy.

## METHODS

**Data Collecting and Processing.** The RNA expression and clinical information of OC samples in the TCGA cohort were downloaded from the UCSC Xena database (<https://gdc.xenahubs.net>, ID: TCGA-OV.htseq\_fpkm, TCGA-OV.GDC\_phenotype, TCGA-OV.survival), and the corresponding mutation information of OC samples was obtained from The Cancer Genome Atlas (TCGA; <https://www.cancer.gov/tcga>). Moreover, The Cancer Immune Atlas (TCIA; <https://tcia.at/>), including genomic immune landscapes of human cancers, supplied the IPS and immunotherapy response of every TCGA OC sample. Combining TCGA and TCIA data sets, 229 OC samples were recruited in this study as a training cohort. The selection criteria and processing of the 229 OC samples included in the TCGA cohort have been previously described.<sup>41</sup>

Furthermore, the GEO cohort was set as a validation cohort, including 240 OC samples. We downloaded data, including gene expression and clinical information, from GSE53963 and GSE26193 via the “GEO query” package.<sup>42</sup> The selection criteria and processing of OC samples in GSE53963 and GSE26193 were described in a previous study.<sup>43–47</sup> The “limma” package<sup>48</sup> eliminated the variability among samples in each GEO data set. Then, we used “sva” package<sup>49</sup> to remove the batch effect from the two GEO data sets and merged the expression data. The complete clinicopathological characteristics of the OC samples included in this study are presented in Table S1.

**Process of DEGs.** Immunophenoscore (IPS) was a superior predictor of response to immune checkpoint blockades. OC samples were divided into high- and low-IPS subgroups based on the median IPS. The “limma” package<sup>48</sup> was used to explore the differentially expressed genes (DEGs) between the high- and low-IPS subgroups with the thresholds of  $\log_2(\text{foldchange}) > 0.5$  and  $\text{adj. } p \text{ value} < 0.05$ . A univariate Cox regression analysis was performed to identify DEGs with OS ( $p < 0.05$ ), in preparation for constructing the prognostic model.

**Construction and Evaluation of the Prognostic Model.** The least absolute shrinkage and selection operator (LASSO) Cox regression (iteration = 1000) could identify the

most critical factors to harness the model’s prediction accuracy and was conducted to avoid overfitting via the “glmnet” package.<sup>50</sup> Five genes were obtained to build the prognostic model, and risk scores were calculated using the following formula:  $\text{risk score} = \sum_{i=1}^n (\text{coef}_i \times \text{exp}_i)$  (Table S2). The median risk score of the TCGA cohort divided OC samples into high- and low-risk subgroups. Principal component analysis (PCA) is a common method of data analysis and is often used to transform high-dimensional data into low-dimensional data via some variables. Every OC sample’s PCA score could be calculated based on the expression of five genes (GLIS2, ISG20, HLA-DOB, KRTCAP3, OCIAD2) via R functions (“prcomp”, “predict”). Kaplan–Meier survival analysis was conducted to compare the OS of subgroups. We applied a time-dependent receiver operating characteristic (ROC) curve to estimate the prognostic precision of the model via the “timeROC” package.<sup>51</sup> Moreover, univariate and multivariate Cox regression analyses were used to determine whether this prognostic model was an independent survival factor impacted by clinical features.

**Establishment of Nomogram.** A nomogram was adopted as an assisted tool to calculate the possibility of one-year, three-year, and five-year OS for every individual based on the risk scores and clinical elements.<sup>52</sup> The ROC curve was used to determine the sensitivity and specificity of the nomogram. The calibration curve was conducted to judge the consistency between predicted survival and actual survival.

**Functional Analysis of the Prognostic Model.** To further explore the primary signaling pathways involved in the prognostic signature, the OC samples were divided into high- and low-risk subgroups based on the median risk score. We then analyzed the DEGs between the high- and low-risk subgroups via the “limma” package<sup>48</sup> with the significance set at  $\text{adj. } p \text{ value} < 0.05$ . Gene Ontology (GO) annotation and Kyoto Encyclopedia of Genes and Genomes (KEGG) pathway enrichment analysis were achieved via the “clusterProfiler” package<sup>53</sup> based on the DEGs. GSEA software (version 4.3.2) was used to analyze the different pathways between the two subgroups. A normal  $p \text{ value} < 0.05$  identified the significant pathways.

**TME Analysis in Two Subgroups.** Single-sample gene set enrichment analysis (ssGSEA) was conducted to estimate the immune cell abundance of each OC patient in TCGA via the “GSVA” package.<sup>54</sup> We then calculated various scores, including tumor purity, immune, stromal, and ESTIMATE scores, via the “estimate” package.<sup>55</sup> Antitumor immunity consists of seven steps, called the cancer-immunity cycle. Tracking Tumor Immunophenotype (TIP) is a meta-server for tracking, analyzing, and visualizing the status of anticancer immunity and the proportion of tumor-infiltrating immune cells, and we downloaded every step for OC patients in TCGA.<sup>56</sup> Then, we compared the different activation of seven steps between the two subgroups.

**Evaluation of TMB and Response to Treatment Efficacy.** The TMB of each OC patient was calculated and compared between the high- and low-risk subgroups. Then, we examined the differences in somatic mutations between the two subgroups via the “maftools” package.<sup>57</sup> Subsequently, we analyzed the effects of immunotherapy and chemotherapy to determine whether the prognostic model influenced therapeutic efficacy. To clarify the impacts on the common drugs in OC, we adopted the “pRRophetic” package<sup>58</sup> to evaluate the half-maximal inhibitory concentration (IC<sub>50</sub>) by ridge

regression based on the Cancer Cell Line Encyclopedia (CCLE) database.

**Statistical Analysis.** R software was used to complete all statistical analyses and graph visualization (v4.2.2; <http://www.r-project.org>). The Wilcoxon rank-sum test was implemented for data not following a uniform distribution and variance. A  $p < 0.05$  was considered to be significant.

## ■ ASSOCIATED CONTENT

### Data Availability Statement

Three data sets: TCGA OC cohort (UCSC XENA, <https://xenabrowser.net/>, ID: TCGA-OV.htseq\_fpkm, TCGA-OV.GDC\_phenotype, TCGA-OV.survival); TCGA-mutation data (TCGA, <https://www.cancer.gov/tcga>); and GEO cohort (GSE26193, GSE53963: <https://www.ncbi.nlm.nih.gov/geo/>)

### Supporting Information

The Supporting Information is available free of charge at <https://pubs.acs.org/doi/10.1021/acsomega.3c04856>.

Complete clinicopathological characteristics of the OC samples included in this study; the gene names and coefficients of 5-gene signature in prognostic model; the clinical features, functional analysis, TME, the expression of immune checkpoints, and drug sensitivity between the high- and low-risk subgroups in the GEO cohort (PDF)

## ■ AUTHOR INFORMATION

### Corresponding Author

Xiaqing Guo – Department of Gynecological Oncology, Shanghai First Maternity and Infant Hospital, School of Medicine, Tongji University, Shanghai 200092, China; Email: [guoxiaqing@51mch.com](mailto:guoxiaqing@51mch.com)

### Authors

Haonan Jiang – Shanghai Key Laboratory of Maternal Fetal Medicine, Shanghai Institute of Maternal Fetal Medicine and Gynecologic Oncology, Shanghai First Maternity and Infant Hospital, School of Medicine, Tongji University, Shanghai 200092, China; [orcid.org/0000-0002-5880-7953](https://orcid.org/0000-0002-5880-7953)

Guzhanuer Awuti – Shanghai Key Laboratory of Maternal Fetal Medicine, Shanghai Institute of Maternal Fetal Medicine and Gynecologic Oncology, Shanghai First Maternity and Infant Hospital, School of Medicine, Tongji University, Shanghai 200092, China

Complete contact information is available at:

<https://pubs.acs.org/doi/10.1021/acsomega.3c04856>

### Author Contributions

H.J. and X.G. conceptualized and designed this study. H.J. performed and achieved the bioinformatics analysis. G.A. collected the data and wrote the original draft preparation. X.G. revised the manuscript and guided the whole analysis. All authors contributed to the article and approved the submitted version.

### Notes

The authors declare no competing financial interest.

## ■ ACKNOWLEDGMENTS

This study was sponsored by the Natural Science Foundation of Shanghai (No. 21ZR1450600) and the Shanghai Sailing Program (No. 20YF1438200).

## ■ ABBREVIATIONS

OC	ovarian cancer
OS	overall survival
IPS	immunophenoscore
TCGA	The Cancer Genome Atlas
TCIA	The Cancer Immune Atlas
GEO	Gene Expression Omnibus
DEGs	differentially expressed genes
LASSO	least absolute shrinkage and selection operator
TME	tumor microenvironment
TMB	tumor mutation burden
PD-1	programmed cell death protein 1
CTLA-4	cytotoxic T lymphocyte antigen-4
GLIS2	GLIS family zinc finger 2
ISG20	interferon-stimulated gene 20 protein
HLA-DOB	human leukocyte antigen-DOB
KRTCAP3	keratinocyte-associated protein 3
OCIAD2	ovarian carcinoma immunoreactive antigen-like protein 2
PCA	principal component analysis
ROC	receiver operating characteristic
AUC	area under curve
HR	hazard ratio
CI	confidence interval
GO	gene ontology
KEGG	Kyoto Encyclopedia of Genes and Genomes
GSEA	gene set enrichment analysis
TP53	tumor protein 53
TTN	titin

## ■ REFERENCES

- (1) Sung, H.; Ferlay, J.; Siegel, R. L.; Laversanne, M.; Soerjomataram, I.; Jemal, A.; Bray, F. Global Cancer Statistics 2020: GLOBOCAN Estimates of Incidence and Mortality Worldwide for 36 Cancers in 185 Countries. *Ca-Cancer J. Clin.* **2021**, *71*, 209–249.
- (2) Kuroki, L.; Guntupalli, S. R. Treatment of epithelial ovarian cancer. *BMJ* **2020**, *371*, No. m3773.
- (3) Banerjee, S.; Moore, K. N.; Colombo, N.; Scambia, G.; Kim, B. G.; Oaknin, A.; Friedlander, M.; Lisyanskaya, A.; Floquet, A.; Leary, A.; Sonke, G. S.; Gourley, C.; Oza, A.; González-Martín, A.; Aghajanian, C.; Bradley, W. H.; Holmes, E.; Lowe, E. S.; DiSilvestro, P. Maintenance olaparib for patients with newly diagnosed advanced ovarian cancer and a BRCA mutation (SOLO1/GOG 3004): 5-year follow-up of a randomised, double-blind, placebo-controlled, phase 3 trial. *Lancet Oncol.* **2021**, *22*, 1721–1731.
- (4) Menon, U.; Gentry-Maharaj, A.; Burnell, M.; Singh, N.; Ryan, A.; Karpinskyj, C.; Carlino, G.; Taylor, J.; Massingham, S. K.; Raikou, M.; Kalsi, J. K.; Woolas, R.; Manchanda, R.; Arora, R.; Casey, L.; Dawnay, A.; Dobbs, S.; Leeson, S.; Mould, T.; Seif, M. W.; Sharma, A.; Williamson, K.; Liu, Y.; Fallowfield, L.; McGuire, A. J.; Campbell, S.; Skates, S. J.; Jacobs, I. J.; Parmar, M. Ovarian cancer population screening and mortality after long-term follow-up in the UK Collaborative Trial of Ovarian Cancer Screening (UKCTOCS): a randomised controlled trial. *Lancet* **2021**, *397*, 2182–2193.
- (5) Hwang, W. T.; Adams, S. F.; Tahirovic, E.; Hagemann, I. S.; Coukos, G. Prognostic significance of tumor-infiltrating T cells in ovarian cancer: a meta-analysis. *Gynecol. Oncol.* **2012**, *124*, 192–198.
- (6) Brewer, M.; Angioli, R.; Scambia, G.; Lorusso, D.; Terranova, C.; Panici, P. B.; Raspagliesi, F.; Scollo, P.; Plotti, F.; Ferrandina, G.; Salutati, V.; Ricci, C.; Braly, P.; Holloway, R.; Method, M.; Madiyalakan, M.; Bayever, E.; Nicodemus, C. Front-line chemo-immunotherapy with carboplatin-paclitaxel using oregovomab indirect

immunization in advanced ovarian cancer: A randomized phase II study. *Gynecol. Oncol.* **2020**, *156*, 523–529.

(7) Pujade-Lauraine, E.; Fujiwara, K.; Ledermann, J. A.; Oza, A. M.; Kristeleit, R.; Ray-Coquard, I. L.; Richardson, G. E.; Sessa, C.; Yonemori, K.; Banerjee, S.; Leary, A.; Tinker, A. V.; Jung, K. H.; Madry, R.; Park, S. Y.; Anderson, C. K.; Zohren, F.; Stewart, R. A.; Wei, C.; Dychter, S. S.; Monk, B. J. Avelumab alone or in combination with chemotherapy versus chemotherapy alone in platinum-resistant or platinum-refractory ovarian cancer (JAVELIN Ovarian 200): an open-label, three-arm, randomised, phase 3 study. *Lancet Oncol.* **2021**, *22*, 1034–1046.

(8) Dijkgraaf, E. M.; Santegoets, S. J.; Reyners, A. K.; Goedemans, R.; Wouters, M. C.; Kenter, G. G.; van Erkel, A. R.; van Poelgeest, M. I.; Nijman, H. W.; van der Hoeven, J. J.; Welters, M. J.; van der Burg, S. H.; Kroep, J. R. A phase I trial combining carboplatin/doxorubicin with tocilizumab, an anti-IL-6R monoclonal antibody, and interferon- $\alpha$ 2b in patients with recurrent epithelial ovarian cancer. *Ann. Oncol.* **2015**, *26*, 2141–2149.

(9) Lampert, E. J.; Zimmer, A.; Padgett, M.; Cimino-Mathews, A.; Nair, J. R.; Liu, Y.; Swisher, E. M.; Hodge, J. W.; Nixon, A. B.; Nichols, E.; Bagheri, M. H.; Levy, E.; Radke, M. R.; Lipkowitz, S.; Annunziata, C. M.; Taube, J. M.; Steinberg, S. M.; Lee, J. M. Combination of PARP Inhibitor Olaparib, and PD-L1 Inhibitor Durvalumab, in Recurrent Ovarian Cancer: a Proof-of-Concept Phase II Study. *Clin. Cancer Res.* **2020**, *26*, 4268–4279.

(10) Schoutrop, E.; El-Serafi, I.; Poiret, T.; Zhao, Y.; Gultekin, O.; He, R.; Moyano-Galceran, L.; Carlson, J. W.; Lehti, K.; Hassan, M.; Magalhaes, I.; Mattsson, J. Mesothelin-Specific CAR T Cells Target Ovarian Cancer. *Cancer Res.* **2021**, *81*, 3022–3035.

(11) Zamarin, D.; Burger, R. A.; Sill, M. W.; Powell, D. J., Jr.; Lankes, H. A.; Feldman, M. D.; Zivanovic, O.; Gunderson, C.; Ko, E.; Mathews, C.; Sharma, S.; Hagemann, A. R.; Khleif, S.; Aghajanian, C. Randomized Phase II Trial of Nivolumab Versus Nivolumab and Ipilimumab for Recurrent or Persistent Ovarian Cancer: An NRG Oncology Study. *J. Clin. Oncol.* **2020**, *38*, 1814–1823.

(12) Konstantinopoulos, P. A.; Waggoner, S.; Vidal, G. A.; Mita, M.; Moroney, J. W.; Holloway, R.; Van Le, L.; Sachdev, J. C.; Chapman-Davis, E.; Colon-Otero, G.; Penson, R. T.; Matulonis, U. A.; Kim, Y. B.; Moore, K. N.; Swisher, E. M.; Färkkilä, A.; D'Andrea, A.; Stringer-Reasor, E.; Wang, J.; Buerstatte, N.; Arora, S.; Graham, J. R.; Bobilev, D.; Dezube, B. J.; Munster, P. Single-Arm Phases 1 and 2 Trial of Niraparib in Combination With Pembrolizumab in Patients With Recurrent Platinum-Resistant Ovarian Carcinoma. *JAMA Oncol.* **2019**, *5*, 1141–1149.

(13) Odunsi, K. Immunotherapy in ovarian cancer. *Ann. Oncol.* **2017**, *28*, viii1–viii7.

(14) Charoentong, P.; Finotello, F.; Angelova, M.; Mayer, C.; Efremova, M.; Rieder, D.; Hackl, H.; Trajanoski, Z. Pan-cancer Immunogenomic Analyses Reveal Genotype-Immunophenotype Relationships and Predictors of Response to Checkpoint Blockade. *Cell Rep.* **2017**, *18*, 248–262.

(15) Covre, A.; Coral, S.; Nicolay, H.; Parisi, G.; Fazio, C.; Colizzi, F.; Fratta, E.; Di Giacomo, A. M.; Sigalotti, L.; Natali, P. G.; Maio, M. Antitumor activity of epigenetic immunomodulation combined with CTLA-4 blockade in syngeneic mouse models. *Oncoimmunology* **2015**, *4*, No. e1019978.

(16) Hugo, W.; Zaretsky, J. M.; Sun, L.; Song, C.; Moreno, B. H.; Hu-Lieskovan, S.; Berent-Maoz, B.; Pang, J.; Chmielowski, B.; Cherry, G.; Seja, E.; Lomeli, S.; Kong, X.; Kelley, M. C.; Sosman, J. A.; Johnson, D. B.; Ribas, A.; Lo, R. S. Genomic and Transcriptomic Features of Response to Anti-PD-1 Therapy in Metastatic Melanoma. *Cell* **2016**, *165*, 35–44.

(17) Bejarano, L.; Jordao, M. J. C.; Joyce, J. A. Therapeutic Targeting of the Tumor Microenvironment. *Cancer Discovery* **2021**, *11*, 933–959.

(18) Goodman, A. M.; Sokol, E. S.; Frampton, G. M.; Lippman, S. M.; Kurzrock, R. Microsatellite-Stable Tumors with High Mutational Burden Benefit from Immunotherapy. *Cancer Immunol. Res.* **2019**, *7*, 1570–1573.

(19) Anagnostou, V.; Forde, P. M.; White, J. R.; Niknafs, N.; Hruban, C.; Naidoo, J.; Marrone, K.; Sivakumar, I. K. A.; Bruhm, D. C.; Rosner, S.; Phallen, J.; Leal, A.; Adleff, V.; Smith, K. N.; Cottrell, T. R.; Rhymee, L.; Palsgrove, D. N.; Hann, C. L.; Levy, B.; Feliciano, J.; Georgiades, C.; Verde, F.; Illei, P.; Li, Q. K.; Gabrielson, E.; Brock, M. V.; Isbell, J. M.; Sauter, J. L.; Taube, J.; Scharpf, R. B.; Karchin, R.; Pardoll, D. M.; Chaft, J. E.; Hellmann, M. D.; Brahmer, J. R.; Velculescu, V. E. Dynamics of Tumor and Immune Responses during Immune Checkpoint Blockade in Non-Small Cell Lung Cancer. *Cancer Res.* **2019**, *79*, 1214–1225.

(20) Boichard, A.; Tsigelny, I. F.; Kurzrock, R. High expression of PD-1 ligands is associated with kataegis mutational signature and APOBEC3 alterations. *Oncoimmunology* **2017**, *6*, No. e1284719.

(21) Zhang, L.; Conejo-Garcia, J. R.; Katsaros, D.; Gimotty, P. A.; Massobrio, M.; Regnani, G.; Makrigiannakis, A.; Gray, H.; Schlienger, K.; Liebman, M. N.; Rubin, S. C.; Coukos, G. Intratumoral T cells, recurrence, and survival in epithelial ovarian cancer. *N. Engl. J. Med.* **2003**, *348*, 203–213.

(22) Yao, J.; Lei, P. J.; Li, Q. L.; Chen, J.; Tang, S. B.; Xiao, Q.; Lin, X.; Wang, X.; Li, L. Y.; Wu, M. GLIS2 promotes colorectal cancer through repressing enhancer activation. *Oncogenesis* **2020**, *9*, No. 57.

(23) Yuan, J.; Tan, L.; Yin, Z.; Tao, K.; Wang, G.; Shi, W.; Gao, J. GLIS2 redundancy causes chemoresistance and poor prognosis of gastric cancer based on co-expression network analysis. *Oncol. Rep.* **2019**, *41*, 191–201.

(24) Deymier, S.; Louvat, C.; Fiorini, F.; Cimarelli, A. ISG20: an enigmatic antiviral RNase targeting multiple viruses. *FEBS Open Bio* **2022**, *12*, 1096–1111.

(25) Gao, M.; Lin, Y.; Liu, X.; Li, Y.; Zhang, C.; Wang, Z.; Wang, Z.; Wang, Y.; Guo, Z. ISG20 promotes local tumor immunity and contributes to poor survival in human glioma. *Oncoimmunology* **2019**, *8*, No. e1534038.

(26) Chang, H.; Zhu, Y.; Zheng, J.; Chen, L.; Lin, J.; Yao, J. Construction of a Macrophage Infiltration Regulatory Network and Related Prognostic Model of High-Grade Serous Ovarian Cancer. *J. Oncol.* **2021**, *2021*, No. 1331031.

(27) Naruse, T. K.; Kawata, H.; Inoko, H.; Isshiki, G.; Yamano, K.; Hino, M.; Tatsumi, N. The HLA-DOB gene displays limited polymorphism with only one amino acid substitution. *Tissue Antigens* **2002**, *59*, 512–519.

(28) Giuliani, C.; Sazzini, M.; Bacalini, M. G.; Pirazzini, C.; Marasco, E.; Fontanesi, E.; Franceschi, C.; Luiselli, D.; Garagnani, P. Epigenetic Variability across Human Populations: A Focus on DNA Methylation Profiles of the KRTCAP3, MAD1L1 and BRSK2 Genes. *Genome Biol. Evol.* **2016**, *8*, 2760–2773.

(29) Wu, D.; Yang, X.; Peng, H.; Guo, D.; Zhao, W.; Zhao, C.; Zhou, X. OCIAD2 suppressed tumor growth and invasion via AKT pathway in Hepatocellular carcinoma. *Carcinogenesis* **2017**, *38*, 910–919.

(30) Nagata, C.; Kobayashi, H.; Sakata, A.; Satomi, K.; Minami, Y.; Morishita, Y.; Ohara, R.; Yoshikawa, H.; Arai, Y.; Nishida, M.; Noguchi, M. Increased expression of OCIA domain containing 2 during stepwise progression of ovarian mucinous tumor. *Pathol. Int.* **2012**, *62*, 471–476.

(31) Liu, K.; Cui, J. J.; Zhan, Y.; Ouyang, Q. Y.; Lu, Q. S.; Yang, D. H.; Li, X. P.; Yin, J. Y. Reprogramming the tumor microenvironment by genome editing for precision cancer therapy. *Mol. Cancer* **2022**, *21*, No. 98.

(32) Jardim, D. L.; Goodman, A.; de Melo Gagliato, D.; Kurzrock, R. The Challenges of Tumor Mutational Burden as an Immunotherapy Biomarker. *Cancer Cell* **2021**, *39*, 154–173.

(33) Henkens, M. T.; Stroeks, S.; Raafs, A. G.; Sikking, M. A.; Tromp, J.; Ouwkerk, W.; Hazebroek, M. R.; Krapels, I. P. C.; Knackstedt, C.; van den Wijngaard, A.; Brunner, H. G.; Heymans, S. R. B.; Verdonschot, J. A. J. Dynamic Ejection Fraction Trajectory in Patients With Dilated Cardiomyopathy With a Truncating Titin Variant. *Circ.: Heart Failure* **2022**, *15*, No. e009352.

- (34) Jia, Q.; Wang, J.; He, N.; He, J.; Zhu, B. Titin mutation associated with responsiveness to checkpoint blockades in solid tumors. *JCI insight* **2019**, *4*, No. e127901.
- (35) Zhang, T.; Jia, Y.; Yu, Y.; Zhang, B.; Xu, F.; Guo, H. Targeting the tumor biophysical microenvironment to reduce resistance to immunotherapy. *Adv. Drug Delivery Rev.* **2022**, *186*, No. 114319.
- (36) Reck, M.; Rodríguez-Abreu, D.; Robinson, A. G.; Hui, R.; Csőszi, T.; Fülöp, A.; Gottfried, M.; Peled, N.; Tafreshi, A.; Cuffe, S.; O'Brien, M.; Rao, S.; Hotta, K.; Leiby, M. A.; Lubiniecki, G. M.; Shentu, Y.; Rangwala, R.; Brahmer, J. R. Pembrolizumab versus Chemotherapy for PD-L1-Positive Non-Small-Cell Lung Cancer. *N. Engl. J. Med.* **2016**, *375*, 1823–1833.
- (37) Fourcade, J.; Sun, Z.; Benallaoua, M.; Guillaume, P.; Luescher, I. F.; Sander, C.; Kirkwood, J. M.; Kuchroo, V.; Zarour, H. M. Upregulation of Tim-3 and PD-1 expression is associated with tumor antigen-specific CD8+ T cell dysfunction in melanoma patients. *J. Exp. Med.* **2010**, *207*, 2175–2186.
- (38) O'Malley, D. M.; Neffa, M.; Monk, B. J.; Melkadze, T.; Huang, M.; Kryzhanivska, A.; Bulat, I.; Meniawy, T. M.; Bagameri, A.; Wang, E. W.; Doger de Speville Uribe, B.; Hegg, R.; Ortuzar Felio, W.; Ancukiewicz, M.; Lugowska, I. Dual PD-1 and CTLA-4 Checkpoint Blockade Using Balmstilimab and Zalifrelimab Combination as Second-Line Treatment for Advanced Cervical Cancer: An Open-Label Phase II Study. *J. Clin. Oncol.* **2022**, *40*, 762–771.
- (39) Maruhashi, T.; Sugiura, D.; Okazaki, I. M.; Shimizu, K.; Maeda, T. K.; Ikubo, J.; Yoshikawa, H.; Maenaka, K.; Ishimaru, N.; Kosako, H.; Takemoto, T.; Okazaki, T. Binding of LAG-3 to stable peptide-MHC class II limits T cell function and suppresses autoimmunity and anti-cancer immunity. *Immunity* **2022**, *55*, 912–924.e8.
- (40) Cho, B. C.; Abreu, D. R.; Hussein, M.; Cobo, M.; Patel, A. J.; Secen, N.; Lee, K. H.; Massuti, B.; Hirt, S.; Yang, J. C. H.; Barlesi, F.; Lee, D. H.; Ares, L. P.; Hsieh, R. W.; Patil, N. S.; Twomey, P.; Yang, X.; Meng, R.; Johnson, M. L. Tiragolumab plus atezolizumab versus placebo plus atezolizumab as a first-line treatment for PD-L1-selected non-small-cell lung cancer (CITYSCAPE): primary and follow-up analyses of a randomised, double-blind, phase 2 study. *Lancet Oncol.* **2022**, *23*, 781–792.
- (41) The Cancer Genome Atlas Research Network. Integrated genomic analyses of ovarian carcinoma. *Nature* **2011**, *474*, 609–615.
- (42) Davis, S.; Meltzer, P. S. GEOquery: a bridge between the Gene Expression Omnibus (GEO) and BioConductor. *Bioinformatics* **2007**, *23*, 1846–1847.
- (43) Gentric, G.; Kieffer, Y.; Mieulet, V.; Goundiam, O.; Bonneau, C.; Nemati, F.; Hurbain, I.; Raposo, G.; Popova, T.; Stern, M. H.; Lallemand-Breitenbach, V.; Müller, S.; Cañeque, T.; Rodriguez, R.; Vincent-Salomon, A.; de Thé, H.; Rossignol, R.; Mechta-Grigoriou, F. PML-Regulated Mitochondrial Metabolism Enhances Chemosensitivity in Human Ovarian Cancers. *Cell Metab.* **2019**, *29*, 156–173.e10.
- (44) Mateescu, B.; Batista, L.; Cardon, M.; Gruosso, T.; de Feraudy, Y.; Mariani, O.; Nicolas, A.; Meyniel, J. P.; Cottu, P.; Sastre-Garau, X.; Mechta-Grigoriou, F. miR-141 and miR-200a act on ovarian tumorigenesis by controlling oxidative stress response. *Nat. Med.* **2011**, *17*, 1627–1635.
- (45) Kieffer, Y.; Bonneau, C.; Popova, T.; Rouzier, R.; Stern, M. H.; Mechta-Grigoriou, F. Clinical Interest of Combining Transcriptomic and Genomic Signatures in High-Grade Serous Ovarian Cancer. *Front. Genet.* **2020**, *11*, No. 219.
- (46) Mieulet, V.; Garnier, C.; Kieffer, Y.; Guilbert, T.; Nemati, F.; Marangoni, E.; Renault, G.; Chamming's, F.; Vincent-Salomon, A.; Mechta-Grigoriou, F. Stiffness increases with myofibroblast content and collagen density in mesenchymal high grade serous ovarian cancer. *Sci. Rep.* **2021**, *11*, No. 4219.
- (47) Konecny, G. E.; Wang, C.; Hamidi, H.; Winterhoff, B.; Kalli, K. R.; Dering, J.; Ginther, C.; Chen, H. W.; Dowdy, S.; Cliby, W.; Gostout, B.; Podratz, K. C.; Keeney, G.; Wang, H. J.; Hartmann, L. C.; Slamon, D. J.; Goode, E. L. Prognostic and therapeutic relevance of molecular subtypes in high-grade serous ovarian cancer. *J. Natl. Cancer Inst.* **2014**, *106*, No. dju249.
- (48) Ritchie, M. E.; Phipson, B.; Wu, D.; Hu, Y.; Law, C. W.; Shi, W.; Smyth, G. K. limma powers differential expression analyses for RNA-sequencing and microarray studies. *Nucleic Acids Res.* **2015**, *43*, No. e47.
- (49) Leek, J. T.; Johnson, W. E.; Parker, H. S.; Jaffe, A. E.; Storey, J. D. The sva package for removing batch effects and other unwanted variation in high-throughput experiments. *Bioinformatics* **2012**, *28*, 882–883.
- (50) Gui, J.; Li, H. Penalized Cox regression analysis in the high-dimensional and low-sample size settings, with applications to microarray gene expression data. *Bioinformatics* **2005**, *21*, 3001–3008.
- (51) Blanche, P.; Dartigues, J. F.; Jacqmin-Gadda, H. Estimating and comparing time-dependent areas under receiver operating characteristic curves for censored event times with competing risks. *Stat. Med.* **2013**, *32*, 5381–5397.
- (52) Iasonos, A.; Schrag, D.; Raj, G. V.; Panageas, K. S. How to build and interpret a nomogram for cancer prognosis. *J. Clin. Oncol.* **2008**, *26*, 1364–1370.
- (53) Yu, G.; Wang, L. G.; Han, Y.; He, Q. Y. clusterProfiler: an R package for comparing biological themes among gene clusters. *OMICS: J. Integr. Biol.* **2012**, *16*, 284–287.
- (54) Hänzelmann, S.; Castelo, R.; Guinney, J. GSEA: gene set variation analysis for microarray and RNA-seq data. *BMC Bioinf.* **2013**, *14*, No. 7.
- (55) Yoshihara, K.; Shahmoradgoli, M.; Martínez, E.; Vegesna, R.; Kim, H.; Torres-García, W.; Treviño, V.; Shen, H.; Laird, P. W.; Levine, D. A.; Carter, S. L.; Getz, G.; Stemke-Hale, K.; Mills, G. B.; Verhaak, R. G. Inferring tumour purity and stromal and immune cell admixture from expression data. *Nat. Commun.* **2013**, *4*, No. 2612.
- (56) Xu, L.; Deng, C.; Pang, B.; Zhang, X.; Liu, W.; Liao, G.; Yuan, H.; Cheng, P.; Li, F.; Long, Z.; Yan, M.; Zhao, T.; Xiao, Y.; Li, X. TIP: A Web Server for Resolving Tumor Immunophenotype Profiling. *Cancer Res.* **2018**, *78*, 6575–6580.
- (57) Mayakonda, A.; Lin, D. C.; Assenov, Y.; Plass, C.; Koeffler, H. P. Maftools: efficient and comprehensive analysis of somatic variants in cancer. *Genome Res.* **2018**, *28*, 1747–1756.
- (58) Gleeleher, P.; Cox, N.; Huang, R. S. pRRophetic: an R package for prediction of clinical chemotherapeutic response from tumor gene expression levels. *PLoS One* **2014**, *9*, No. e107468.